Reynolds Number Effects on Shock-Wave Turbulent Boundary-Layer Interactions

C. C. Horstman*
NASA Ames Research Center, Moffett Field, Calif.

G. S. Settles,† I. E. Vas,‡ and S. M. Bogdonoff§
Princeton University, Princeton, N.J.

and

C. M. Hung¶
NASA Ames Research Center, Moffett Field, Calif.

An experiment is described that tests and guides computations of a shock-wave turbulent boundary-layer interaction flow over a 20° compression corner at Mach 2.85. Numerical solutions of the time-averaged Navier-Stokes equations for the entire flowfield, employing various turbulence models, are compared with the data. Each model is evaluated critically by comparisons with the details of the experimental data. Experimental results for the extent of upstream pressure influence and separation location are compared with numerical predictions for a wide range of Reynolds numbers and shock-wave strengths.

Nomenclature

A^+ = Van Driest damping parameter
C_f = skin-friction coefficient
K = von Karman constant
M = Mach number
p = pressure
p^+ = dimensionless pressure gradient, $(\rho_w \mu_w (dp_w/dx)/(\rho_w \tau_w)^{3/2}$
R = reattachment location
Re = Reynolds number
S = separation location
T = temperature
u = component of velocity parallel to model surface
x = distance along model surface measured from corner
y = distance normal to model surface
y^+ = dimensionless distance from wall, $y(\rho_w \tau_w)^{1/2}/\mu_w$
α = corner angle
β = dimensionless pressure gradient, $\delta_i^*(dp_w/dx)/\tau_w$
δ = boundary-layer thickness
δ_i^* = kinematic boundary-layer displacement thickness
δ^* = boundary-layer displacement thickness
Δx_p = upstream pressure influence parameter, Fig. 13
Δx_s = upstream extent of separation, Fig. 13
ϵ = eddy viscosity
θ = boundary-layer momentum thickness
μ = molecular viscosity
ρ = density
τ = total shear stress

Subscripts

0 = initial boundary-layer conditions, ahead of the interaction
w = wall
∞ = freestream conditions, ahead of the interaction
δ_0 = based on δ_0

Received Jan. 11, 1977; presented as Paper 77-42 at the AIAA 15th Aerospace Sciences Meeting, Los Angeles, Calif., Jan. 24-26, 1977; revision received April 18, 1977.

Index categories: Boundary Layers and Convective Heat Transfer – Turbulent; Supersonic and Hypersonic Flow; Computational Methods.

*Assistant Chief, Experimental Fluid Dynamics Branch. Associate Fellow AIAA.

†Research Staff Member, Gas Dynamics Laboratory. Member AIAA.

‡Senior Research Engineer and Lecturer, Gas Dynamics Laboratory. Associate Fellow AIAA.

§Professor and Chairman, Department of Aerospace and Mechanical Sciences. Fellow AIAA.

¶Consultant, DCW Industires. Member AIAA.

Introduction

WITH recent developments in computer technology along with advances in computational fluid dynamics, routine computations of shock-wave turbulent boundary-layer interactions are now possible. Examples of these computations, solving the full time-averaged Navier-Stokes equations with various proposed turbulence models, are included in Refs. 1-7. The solutions[1-7] have met with various degrees of success and show that the turbulence models applicable to zero pressure gradient boundary layers are not appropriate for shock-wave boundary-layer interaction flows. The use of an advanced two-equation turbulence model[1] and modifed two-layer eddy viscosity models[2-7] indicated some improvement in predicting the experimental results. However, for most of these comparisons, the lack of sufficiently detailed experimental data precludes verification of these turbulence models. The few experiments[6,7] in which sufficient data have been obtained might have the added complication of separation unsteadiness which could have a significant influence on the resulting flowfield. To test adequately the numerical similation of a complex interaction flow, the experiment should include detailed flowfield measurements as well as surface measurements.[8] The tests also should be conducted for a wide range of Reynolds numbers and shock-wave strengths. One such experimental program is in progress at the Gas Dynamics Laboratory of Princeton University.

This paper combines experimental and numerical methods to guide and verify turbulence modeling for supersonic shock-wave boundary-layer-interaction flows. The experimental documentation of the flow over a two-dimensional 20° compression corner model at a Mach number 2.85 is described first. Detailed measurements, consisting of surface pressure, skin friction, and boundary-layer profiles of pitot and static pressure and total temperature were obtained at finely spaced intervals along the surface of the model. Secondly, experimental results, including previously obtained data for a

24° compression corner,[9,10] are compared with computations using the time-dependent, time-averaged Navier-Stokes equations employing various turbulence models to describe the shear stress. Each model is evaluated critically and its deficiencies are described. Finally, experimental results on the extent of upstream pressure influence and separation location are compared with numerical predictions for a wide range of Reynolds numbers and shock-wave strengths.

Description of Experiment

Facility

The experimental part of this study was carried out in the Princeton University high-Reynolds-number, 8×8 in. supersonic blowdown wind tunnel. A sketch of this facility appears in Fig. 1. The compression corner test models were mounted on the floor of the 20.3-cm², constant-area duct in tunnel section 2, at a point 1.17-m downstream of the nozzle throat. The present tests were performed at a uniform freestream Mach number of 2.85, a stagnation pressure of 6.8 atm (100 psia), and a stagnation temperature of 280 K(±2%). The corresponding freestream unit Reynolds number is 6.3×10^7/m.

Test Models

Both 20° and 24° compression corner test models (see Fig. 1) were constructed of solid brass. The width of each compression ramp (15.2 cm) allowed gaps at the sides for the passage of the sidewall boundary layers. Aerodynamic fences were attached to the ramp sides to isolate further the shock-boundary-layer interaction from sidewall boundary-layer influences.

Details of the 24° compression corner model, as well as test results, are treated in an earlier publication.[10] The 20° model, for which results are presented here for the first time, was instrumented with 47 surface-pressure taps and 3 surface thermocouples. Pressure taps were arranged so as to sense transverse as well as longitudinal pressure gradients. Two such taps were located in the compression corner itself.

Test Procedure and Accuracy

Detailed flowfield surveys were carried out with probes that were inserted through the tunnel ceiling, thus approaching the 20° and 24° compression corner interactions from above. In both cases, all of the probe surveys were made in a vertical streamwise plane intersecting the model 1.27 cm to the right of its centerline.

The flowfields under consideration were surveyed with static pressure, pitot pressure, total temperature, and Preston tube probes. The pitot probes had flat tips of 0.18-mm height. Miniature cone-tipped needle probes, 0.8 mm in diameter and 1.5-cm long, were used for static pressure measurements. Total temperature was measured using 0.1-mm-diam fine-wire probes. A reverse pitot probe tip was used in obtaining reversed-flow data in separated flow regions. Preston tube measurements were made with tubes ranging in daimeter from 1.6 to 3.2 mm. Details of the data reduction techniques employed to obtain surface skin friction are given in Ref. 9.

Visualizations of the interaction flow patterns were obtained by way of the standard shadowgraph and monochrome schlieren techniques, and also by some specialized color schlieren methods. Surface flow patterns were obtained using the surface-dot technique and the kerosene-graphite technique.[9,10]

The impact of probe interference with the flow was assessed in a preliminary series of tests in which the surface pressure, flow pattern, and schlieren image were monitored carefully for changes when probes were introduced into the flowfield. Probe interference was found not to be significant.

Mean streamwise velocity profiles were derived from the combination of pitot pressure, static pressure, and total temperature profiles at each survey station. The static pressure profiles are believed to be accurate to within ±4% except in the immediate vicinity of the shock-wave system. Estimated accuracies of the pitot and total temperature profiles are ±2% and ±1½%, respectively. Errors in the mean streamwise velocity profiles derived from these measurements are believed to be generally within ±5% except in the separated zone where the measured velocities are extremely small.

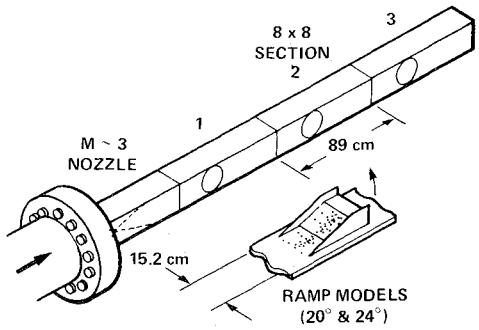

Fig. 1 Sketch of 8- by 8-in. supersonic wind tunnel and test model.

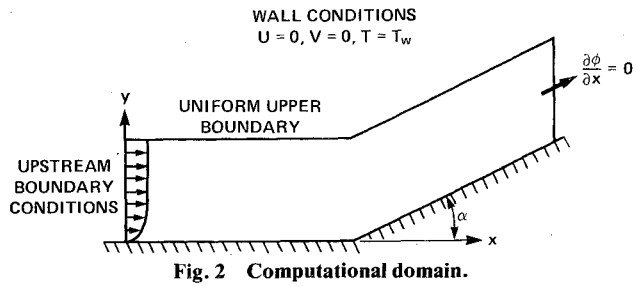

Fig. 2 Computational domain.

Description of Numerical Simulation

Computational Domain and Boundary Conditions

The mass-averaged Navier-Stokes equations for compressible flow were used to predict the flow throughout the

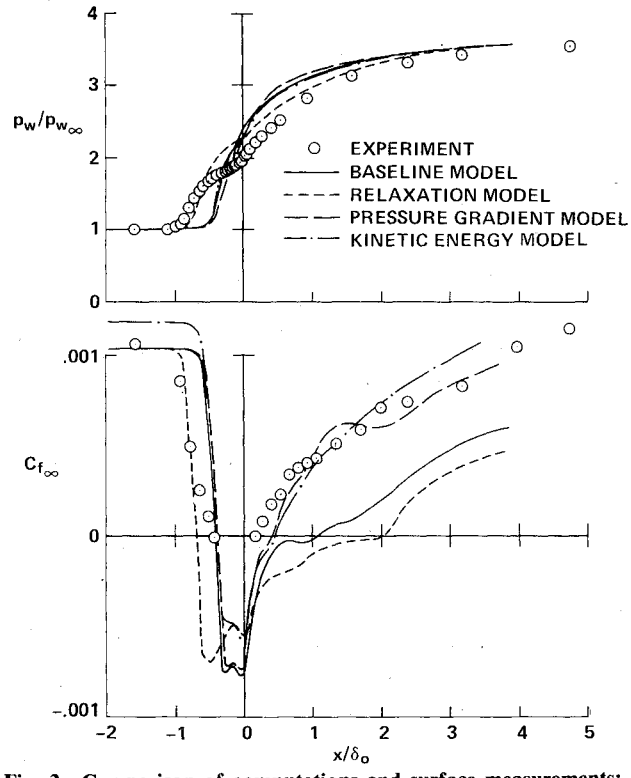

Fig. 3 Comparison of computations and surface measurements; $\alpha = 20°$, $Re_{\delta_0} = 1.65\times10^6$.

interaction region. The turbulent Reynolds stress and heat flux terms in these equations are related to the mean flow gradients of velocity and temperature by eddy transport coefficients that are added to the molecular-transport coefficients. The resulting equations are described in Ref. 3.

The computation domain and the appropriate boundary conditions are shown in Fig. 2. The mesh is equally spaced in the x direction; in the y direction, a fine, geometrically stretched mesh spacing is used near the wall for resolving the viscous layer with a coarse, equally spaced mesh in the outer region where viscous effects are negligible. A total of 50 mesh points in the x direction and 32 points in the y direction (with 23 points in the boundary layer) were used for the present computations. The upper boundary is located approximately three boundary-layer thicknesses above the wall to insure uniform freestream conditions at this height, and the upstream boundary is located several boundary-layer thicknesses ahead of the interaction region. The initial boundary-layer thicknesses varied from 1.6 to 2.4 cm, depending on the Reynolds number of the flow. Near the wall, the first mesh point was placed so as to insure its inclusion within the viscous sublayer ($y^+ < 7$), both upstream and downstream of the compression corner. These vertical distances varied from 0.18×10^{-3} to 0.72×10^{-3} cm, depending on the Reynolds number of the flow. In the x direction two mesh spacings were used, 0.26 and 0.49 cm. The larger mesh spacing was used to examine the influence of extending the upstream and downstream boundaries. No differences were observed in the computed flowfields using the two mesh spacings. For the two fully documented flowfields, $\alpha = 20°$ and 24°, the experimentally determined lengths of the separated regions were 1.5 and 4.1 cm, respectively. Thus, the x direction mesh spacing should be sufficient to resolve the details of the two separated regions.

The upstream boundary conditions were prescribed by a combination of uniform freestream conditions and a boundary-layer program modified by Marvin and Sheaffer[11] to calculate turbulent boundary layers. The boundary-layer program was run for an x distance that insured a match of the experimentally and numerically determined displacement thicknesses for each case. The downstream boundary is positioned far enough aft of the compression corner that all of the gradients in the flow direction can be set to zero. Though this condition is not exact, the boundary layer and outer flowfield in the vicinity of this boundary are mostly supersonic; hence, it is not expected that this condition will introduce significant errors in the region of interest. This was verified by moving the location of this downstream boundary and observing substantially unchanged numerical results. The upper boundary is specified by the freestream conditions. The wall surface is assumed impermeable, and no-slip boundary conditions are applied with a constant wall temperature.

The numerical method and special numerical procedures used in the calculation presented herein are described in detail in Refs. 3 and 12. A new algorithm described by MacCormack[13] also was employed to speed up the computational time required for each solution. Computation times to achieve fully converged solutions on a CDC 7600 varied from 5 min for compression corner angles of 10°, to 12 min for corner angles of 24°.

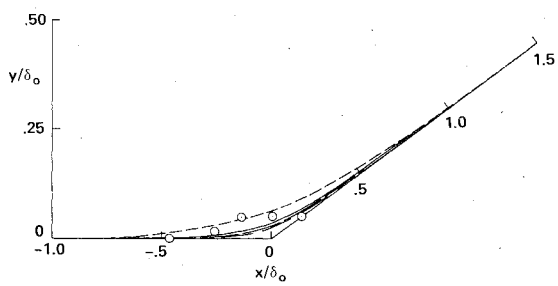

Fig. 4 Comparison of computations and measurements of the zero-velocity line; $\alpha = 20°$, $Re_{\delta_0} = 1.65 \times 10^6$.

Turbulence Models

Four turbulence models were used for the present computations. Each of the first three models is a two-layer eddy viscosity model using the Prandtl mixing length concept for the inner region and Clauser's defect law in the outer region. In the inner layer,

$$\epsilon_{\text{inner}} = \rho \ell^2 \left[\left(\frac{\partial u}{\partial y} \right)^2 + \left(\frac{\partial v}{\partial x} \right)^2 \right]^{1/2} \tag{1}$$

where

$$\ell = Ky[1 - \exp(-y^+/A^+)] \tag{2}$$

with $K = 0.4$ and $A^+ = 26$. In the outer region,

$$\epsilon_{\text{outer}} = 0.0168 \rho u_e \delta_i^* / I \tag{3}$$

where I is the Klebanoff intermittency correction factor

$$I = [1 + 5.5(y/\delta)^6] \tag{4}$$

The turbulent heat flux was expressed in terms of the eddy viscosity assuming a turbulent Prandtl number equal to 0.90. The baseline model is the preceding two-layer eddy-viscosity model with no corrections for pressure gradient. This model was consistent with that used in the boundary-layer code to describe the input conditions as mentioned previously. The second, a relaxation model, is a modification to the baseline model to account for upstream turbulence history effects:

$$\epsilon = \epsilon_{eq} - (\epsilon_{eq} - \epsilon_0) \exp[-(x - x_0)/\lambda] \tag{5}$$

where

ϵ = turbulence dynamic eddy viscosity
ϵ_{eq} = local equilibrium eddy viscosity evaluated from Eqs. (1) and (3)
ϵ_0 = eddy viscosity at upstream location x_0
λ = relaxation length

This model has been used by many investigators[3-6] to solve separated flow problems. Basically, this model increases the extent of the upstream influence and separation bubble size, resulting in larger pressure plateaus. For previous comparisons with experimental data, this modification was found necessary to achieve agreement with experimental pressure distributions. Both of these models are described in detail by Hung and MacCormack.[3] For the present computations the relaxation length, which describes the exponential decay of

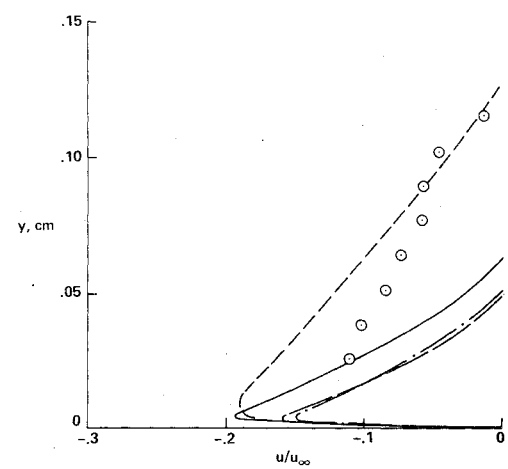

Fig. 5 Comparison of computations and measurements of a reversed flow velocity profile; $\alpha = 20°$, $Re_{\delta_0} = 1.65 \times 10^6$.

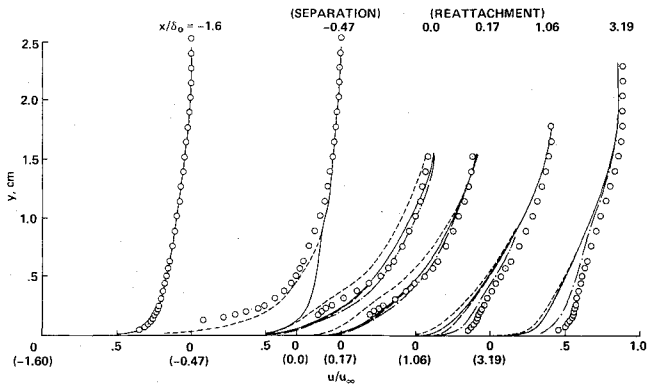

Fig. 6 Comparison of computations and velocity profile measurements at selected x stations; $\alpha = 20°$, $Re_{\delta_0} = 1.65 \times 10^6$.

the eddy viscosity distribution, was assumed to be equal to the local boundary-layer thickness. The third, a pressure gradient model, is the baseline model with modifications to the von Karman and van Driest constants to account for the effects of both adverse pressure gradient and turbulence memory.

The expression for A^+ becomes

$$A^+(x) = 26/[1 + 30.18\,\overline{p^+(x)}] \tag{6}$$

where

$$\overline{p^+(x)} = \int_{x-2\lambda\delta}^{x} w(\xi)\,p^+(\xi)\,d\xi \tag{7}$$

$$w(\xi) = (1/\sqrt{2\pi\sigma})\exp\{-[\xi-(x-\lambda\delta)]^2/2\sigma^2\} \tag{8}$$

$$\sigma = \lambda\delta/3 \tag{9}$$

The expression for K becomes

$$K(x) = 0.4 + 0.182257\{1 - \exp[-0.32068\,\overline{\beta(x)}]\} \tag{10}$$

where $\overline{\beta(x)}$ is computed using Eqs. (7-9) by replacing $p^+(x)$ by $\beta(x)$. This model, developed by Horstman,[14] was shown to be very successful in predicting attached boundary-layer flows but had not been applied to separated flows. For the present computations the lag-length parameter, which describes the turbulence memory effects due to pressure gradient, was assumed to be equal to the local boundary-layer thickness. The results of Ref. 14 indicate that this value of the lag-length parameter should be appropriate for flows with separation. Absolute values of τ_w were employed to define p^+ and β.

The fourth model is a one-equation eddy viscosity model which employs a differential equation to describe the turbulent kinetic energy and an algebraic length scale. This model was developed for incompressible flows by Glushko[15] and extended to compressible flows by Rubesin.[16] Details of this model are described by Viegas and Coakley.[17] For the present computations the constants employed are those suggested by Viegas and Coakley[17] (Model BlaO) which gave good agreement for compressible flat-plate flows.

Results and Discussion

Experiment

The previously obtained experimental results for the 24° compression corner, which are reproduced here for comparison with the numerical computations, were described in detail elsewhere.[9,10] The results for the 20° compression corner are compared with the computations in Figs. 3-6. The comparison is described in the following section.

The incoming boundary layer in the 20° experiment was found to have the following thickness parameters: $\delta_0 = 23.9$ mm, $\delta_0^* = 7.33$ mm, and $\theta_0 = 1.19$ mm. In transformed coordinates, its profile compared closely with the known form of an equilibrium turbulent boundary layer in incompressible flow.

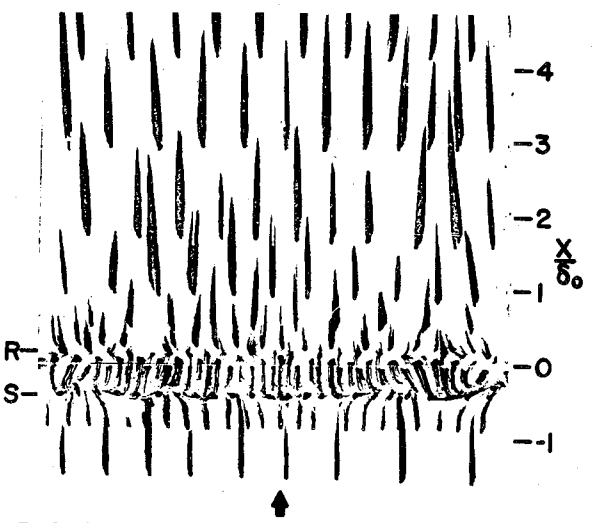

Fig. 7 Surface-streak flow pattern on the 20° compression corner model.

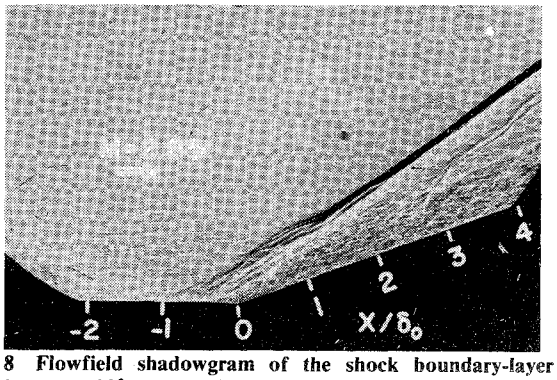

Fig. 8 Flowfield shadowgram of the shock boundary-layer interaction at the 20° compression corner.

The surface streak pattern shown in Fig. 7 clearly indicates the locations of the flow separation S and the reattachment R lines relative to the 20° compression corner ($x/\delta_0 = 0$). The directions of the streaks between these two lines illustrate the fact that the flow near the model surface is in a direction opposite to that of the freestream. Also, the separation and reattachment lines in Fig. 7 are found to be essentially straight over more than 90% of the model's span, supporting the assumption that the interaction is two dimensional.

Two dimensionality also is supported strongly by the favorable comparison of upstream influence and other parameters with the trends of data obtained from smaller-angle compression corner flows of known two dimensionality.[9] Relatively small transverse surface pressure variations and the interchangeability of aerodynamic fences further support the assumption of two-dimensional flow, as does the 12:1 aspect ratio of the separated flow region.

Figure 8 presents a typical microsecond-exposure shadowgram of the shock/boundary-layer interaction caused by the 20° compression corner. (This photograph was made without aerodynamic fences in place.) The incoming turbulent boundary layer is seen to undergo a fan of compression waves originating near the surface at about $x/\delta_0 = \frac{1}{2}$. Outside the boundary layer this compression fan coalesces into a single oblique shock wave. The outgoing boundary layer has a reduced thickness and a visibly greater activity of turbulent density fluctuations. The apparently weaker oblique shock lying parallel to and $1/2\delta_0$ downstream of the main shock is actually only an artifact caused by the intersection of the main shock with the wind-tunnel windows.

A sequence of several consecutive spark shadowgrams was obtained during a single test run in order to evaluate the magnitude of any unsteadiness in the flowfield. Motions and ripples of the flow pattern were noticed only to the extent of $1/10\delta_0$ or less. The scale of these fluctuations is 2% or less of the overall scale of the interaction, and thus is not considered further.

The 20° compression corner surface pressure distribution, as given in Fig. 3, reaches the theoretical inviscid level for a 20°, $M=2.85$ turn between $x/\delta_0=4$ and 5. The well-known "kink" in the distribution, indicative of flow separation, is found near the compression corner. However, no outright pressure "plateau" appears. The skin-friction coefficient, as determined from Preston tube readings, is zero at longitudinal points corresponding to the separation and reattachment line locations in Fig. 7.

The shape and location of the zero mean velocity line in the separated region is shown in Fig. 4. As in the 24° corner tests, present 20° results show a greater distance from corner-to-separation than from corner-to-reattachment. However, the 20° zero-velocity line is more convex, or bubble-shaped, than the nearly linear zero-velocity line of the 24° compression corner flow. The reversed-flow velocity profile at the compression corner, shown in detail in Fig. 5, tends toward a maximum velocity of $0.11u_\infty$ near the model surface.

Finally, mean streamwise velocity profiles throughout the 20° flowfield are summarized in Fig. 6. The incoming equilibrium turbulent boundary layer is retarded severely by the adverse pressure gradient of the interaction, but recovers rapidly downstream of the reattachment line. The velocity profile at $x/\delta_0=3.19$, although still somewhat retarded between $0.1<y/\delta_0<0.5$, is otherwise quite similar to the incoming profile. Throughout the region downstream of the compression corner, small gradients in static pressure normal to the model surface were found. These gradients decayed somewhat in the downstream direction, but had not disappeared completely at the downstream end of the compression ramp. Similar results were observed earlier in the 24° compression corner tests.[10]

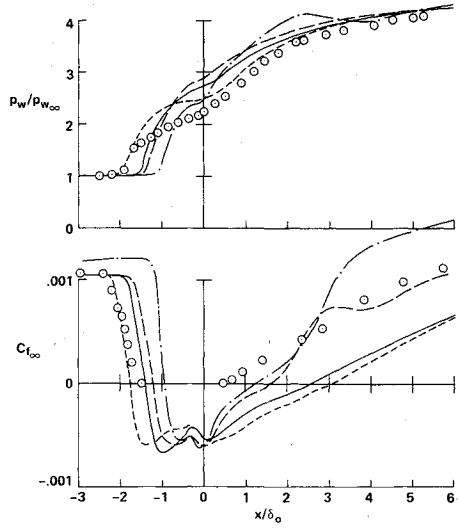

Fig. 9 Comparison of computations and surface measurements; $\alpha=24°$, $Re_{\delta_0}=1.33\times10^6$.

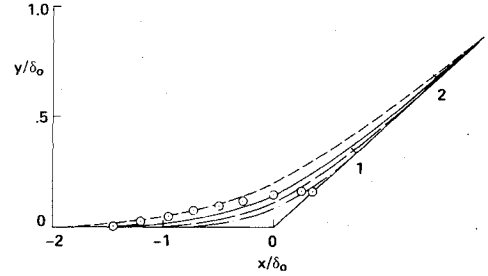

Fig. 10 Comparison of computations and measurements of the zero-velocity line; $\alpha=24°$, $Re_{\delta_0}=1.33\times10^6$.

Comparison of Numerical Simulation and Experiment

Results of the computation solving the complete time-averaged Navier-Stokes equations using the various turbulence models are compared with the present experimental data for the 20° ramp in Figs. 3-6 and with previous data[9,10] for the 24° ramp in Figs. 9-12. Comparisons are made for the wall pressure and skin-friction distributions (Figs. 3 and 9), zero-velocity line shapes (Figs. 4 and 10), reversed mean velocity profiles at the corner (Figs. 5 and 11), and several mean velocity profiles throughout the flowfield (Figs. 6 and 12). (The symbol key shown in Fig. 3 indicating the various computations is also appropriate for the remaining figures.) In general, the comparisons of the various computations and the data show similar results for the two ramp angles, although the extent of separation is significantly different for the two flowfields.

The computations employing the baseline model predict the qualitative features of the two flows reasonably well, considering the simplicity of the turbulence model, but a closer examination of the comparisons points out the deficiencies of the computations. The overall pressure rise is predicted well but the locations of the initial rise in pressure are not. Also the computations do not predict a pressure "plateau." Comparing the skin-friction results, the computations predict the locations of separation well but do not predict the reattachment locations and substantially underpredict the skin friction downstream of reattachment. Comparing the zero-velocity line shapes, the computations using the baseline model underpredict the initial heights and give the incorrect shapes. These results are consistent with the lack of a predicted pressure plateau; a larger initial separation bubble size would result in a pressure plateau. Comparison of the velocity distributions in the separation bubble shows that the computations agree reasonably well with the data but show a larger negative velocity close to the wall. The remaining comparisons with the experimental velocity distributions show general disagreement except for the undisturbed upstream profile. The large disagreements far downstream of the interaction region could have serious consequences for predicting a flow where more than one interaction takes place.

Previous authors[2,3] have used the relaxation model to improve the numerical simulation of separated corner flows. Their comparisons were based primarily on the experimental pressure distributions and separation location. The present computations employing the relaxation model also show an improvement in predicting the pressure distribution. Good agreement also is achieved for the velocity profiles at separation. However, downstream of the corner the results obtained with this model are not as good as those obtained with the baseline model. For the velocity profile comparisons (Figs. 6 and 12), the results obtained using the various turbulence models are shown only where they differ from the results using the baseline model. It also is noted that the computations overpredict the pressure plateau level. Larger values of the relaxation length do not alter this level, although they do increase the extent of upstream influence. Previous comparisons[2,3] with experimental data obtained at similar Mach numbers but at much lower Reynolds numbers ($Re\delta_0=0.14\times10^6$) have shown good agreement between the calculated and measured plateau pressure levels. Perhaps this agreement was fortuitous.

The computations employing the pressure gradient model do an excellent job in predicting the skin-friction levels far downstream of reattachment and are in better agreement with the experiments than the baseline model so far as the location of reattachment is concerned. However, the computed velocity profiles are still in substantial disagreement with the

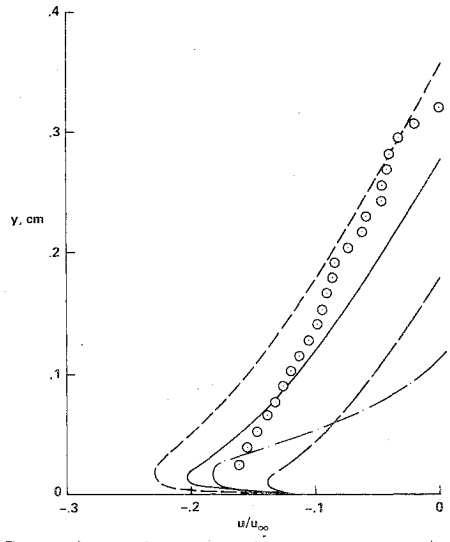

Fig. 11 Comparison of computations and measurements of a reversed flow velocity profile; $\alpha = 24°$, $Re_{\delta_0} = 1.33 \times 10^6$.

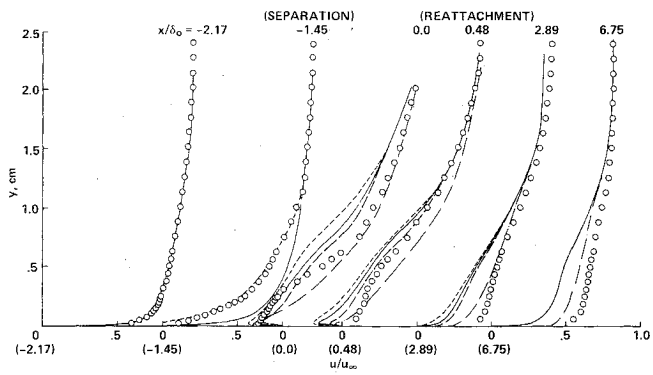

Fig. 12 Comparison of computations and velocity profile measurements at selected x stations; $\alpha = 24°$, $Re_{\delta_0} = 1.33 \times 10^6$.

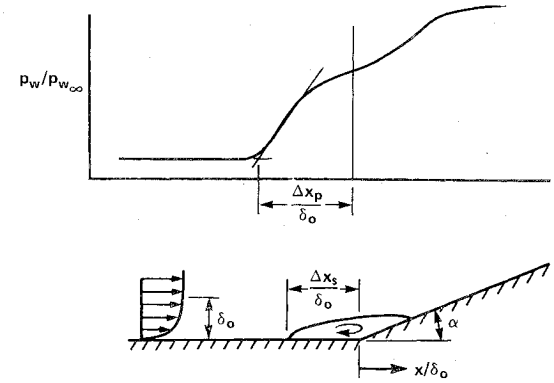

Fig. 13 Definition of geometric distances.

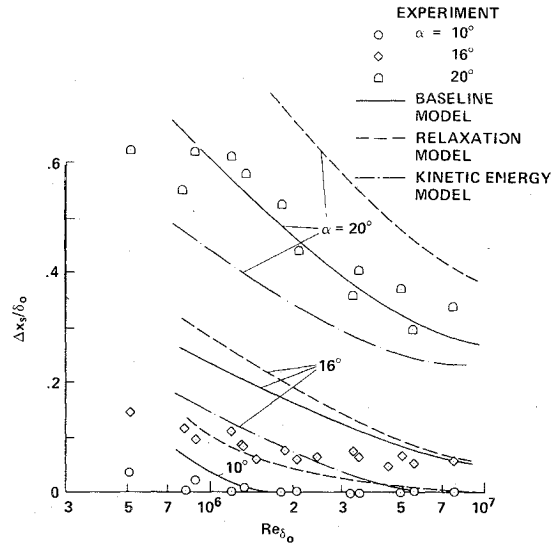

Fig. 14 Comparison of computations and measurements of the effect of Reynolds number on separation length.

experimental results and only slightly better than those for the baseline model. This is because the pressure gradient corrections only were applied to the turbulence model in the region close to the wall. During this investigation, attempts have been made to alter the turbulence model in the outer region of the boundary layer to account for pressure gradient effects, but with little improvement.

Computations employing the kinetic energy turbulence model show significant improvement over the baseline model results at and downstream of reattachment. Both the predicted skin-friction levels and velocity profiles are in better agreement with the experimental results than the baseline model predictions. However, in the separated zone, the kinetic energy model results predict a much smaller bubble height and extent of upstream pressure influence than experimentally measured. Previous results[17] employing the kinetic energy model for calculating separated flows also showed improved agreement with experimental results downstream of reattachment. Although the computations may be satisfactory for engineering purposes, it is clear that the details of the flowfield are not being simulated correctly numerically.

The preceding comparisons clearly point out the advantages of a fully documented experiment for testing a turbulence model. Although some turbulence models may do an excellent job of predicting one particular type of measurement, such as the wall pressure or skin-friction distribution, none of them adequately predicts the velocity distribution throughout the flowfield for these particular experimental data. These results indicate that the four turbulence models considered all have significant deficiencies, although the baseline model does predict the separation location correctly and the pressure gradient model predicts skin friction reasonably well. The turbulent kinetic energy model aso predicts skin friction reasonably well in addition to being the only model considered to show improved agreement with the downstream velocity profiles. In the separated zone, it is difficult to choose a best model because the differences obtained using the various models are probably within the accuracy of the data except for the separation and reattachment locations. The primary disagreement between the computations and the experiment is found in the flowfield at reattachment and downstream. The one-equation kinetic energy model shows the best agreement in this region. Perhaps a two-equation model which calculates the length scale such as employed by Wilcox[1] would provide better agreement with the experiment.

Prediction of Reynolds Number and Corner Angle Effects

Since the previous detailed comparisons indicate that the separation location can be predicted reasonably well, it is of interest to test this prediction against the Princeton experiments for a wide range of Reynolds numbers and corner angles. Separation locations and other data have been obtained[9,18] for variations in Reynolds number based on boundary-layer thickness from 0.5 to 8.0×10^6 and for corner angle variations from 10° to 24°. Solutions employing the baseline, relaxation, and kinetic energy turbulence models have been obtained for the range of experimental test conditions. Two calculated parameters are compared with the experimental test results – the extent of upstream pressure

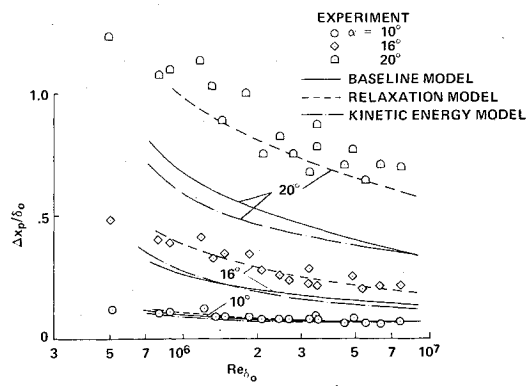

Fig. 15 Comparison of computations and measurements of the effect of Reynolds number on the extent of upstream pressure influence.

influence Δx_p and the extent of separation Δx_s ahead of the corner. These parameters are defined in Fig. 13.

The computed extent of separation using the baseline model as a function of Reynolds number and corner angle is compared with the experimental values in Fig. 14. For a corner angle of 20° there is excellent agreement over the entire Reynolds number range. For the lower corner angles, the computations predict a larger separation distance than was found experimentally. Also shown are the results using the relaxation and kinetic energy models. These results show similar Reynolds number trends but the relaxation model results overpredict the data and the kinetic energy model results underpredict the data at $\alpha = 20°$.

The computed upstream extent of the interaction pressure rise is compared with experimental values in Fig. 15. It is seen that trends with Reynolds number are predicted well with all three models but only the relaxation model predicts the correct magnitude. Previous comparison with other experimental data[2-4] have shown that larger relaxation lengths (up to 10δ) were required to match experimental pressure data. A few computations have been obtained for the present conditions at relaxation lengths up to 5δ. The resulting values of Δx_p were increased up to 50%.

Concluding Remarks

A detailed experimental documentation of the mean flow throughout a shock-wave, boundary-layer interaction has been presented. These data were of sufficient detail and quality to assess the validity of numerical simulations and to guide turbulence model changes.

Numerical solutions, employing the full time-averaged Navier-Stokes equations along with various eddy-viscosity models, have been compared with the details of the measured flowfields. Computations employing the baseline turbulence model gave reasonable agreement with the experiment for the location of separation and the overall pressure rise. However, the reattachment location and the flowfield downstream of reattachment were in significant disagreement with the measurements. Use of a relaxation model slightly improved the agreement with the experiment at separation but gave worse results downstream. Inclusion of a pressure gradient correction provided better agreement with experimental skin-friction results but failed correctly to predict the downstream flowfield profiles. Each algebraic eddy-viscosity model tested here appeared seriously to overestimate the downstream distance required for the recovery of the boundary layer from the effects of the interaction. The one-equation kinetic energy model showed significant improvement over the algebraic models in this respect but did not predict correctly the details of the separated flowfields. The authors believe that further improvement will be obtained only with the use of more advanced turbulence models that have, if possible, a more realistic relationship to the physics of turbulence itself.

Numerical solutions employing three of the present turbulence models also have been compared with the experimental results on the extent of upstream pressure influence and separation over a wide range of Reynolds numbers and corner angles. It has been shown, at least for large corner angles, that the effects of Reynolds number are predicted correctly. Unfortunately, the numerical results are not well suited for the determination of incipient separation angles, which are functions of the grid spacing; and that step has not been attempted here.

Acknowledgment

The experimental studies were carried out at the Gas Dynamics Laboratory, Princeton University, with the support of NASA Ames Research Center, Grant NSG-2114, and the Air Force Office of Scientific Research, Contract F44620-75-C-0080.

References

[1] Wilcox, D.C., "Numerical Study of Separated Turbulent Flows," *AIAA Journal,* Vol. 13, May 1975, pp. 555-556.

[2] Shang, J.S. and Hankey, W.L., "Numerical Solution for Supersonic Turbulent Flow Over a Compression Ramp," *AIAA Journal,* Vol. 13, Oct. 1975, pp. 1368-1374.

[3] Hung, C.M. and MacCormack, R.W., "Numerical Simulation of Supersonic and Hypersonic Turbulent Compression Corner Flows," *AIAA Journal,* Vol. 15, March 1977, pp. 410-416.

[4] Baldwin, B.S. and MacCormack, R.W., "Modifications of the Law of the Wall and Algebraic Turbulence Modeling for Separated Boundary Layers," AIAA Paper 76-350, San Diego, Calif., July 1976.

[5] Deiwert, G.S., "Computation of Separated Transonic Turbulent Flows," *AIAA Journal,* Vol. 14, June 1976, pp. 735-740.

[6] Mateer, G.G., Brosh, A., and Viegas, J.R., "A Normal Shock-Wave Turbulent Boundary-Layer Interaction at Transonic Speeds," AIAA Paper 76-161, Washington, D.C., Jan 1976.

[7] Marvin, J.G., Horstman, C.C., Rubesin, M.W., Coakley, T.J., and Kussoy, M.I., "An Experimental and Numerical Investigation of Shock-Wave-Induced Turbulent Boundary-Layer Separation At Hypersonic Speeds," *AGARD Conference Proceedings on Flow Separation,* May 1975, No. 168.

[8] Marvin, J.G., "Experiments Planned Specifically for Developing Turbulence Models in Computations of Flow Fields Around Aerodynamic Shapes," Paper 14, *AGARD Specialists' Meeting on Numerical Methods and Wind-Tunnel Testing,* June 23-24, 1976, Von Karman Institute Rhode-St-Genese, Belgium.

[9] Settles, G.S., "An Experimental Study of Compressible Turbulent Boundary-Layer Separation at High Reynolds Numbers," Ph.D. Thesis, 1975, Department of Aerospace and Mechanical Sciences, Princeton University.

[10] Settles, G.S., Vas, I.E., and Bogdonoff, S.M., "Details of a Shock-Separated Turbulent Boundary Layer at a Compression Corner," *AIAA Journal,* Vol. 14, Dec. 1976, pp. 1709-1715.

[11] Marvin, J.G. and Sheaffer, Y.S., "A Method for Solving the Nonsimilar Boundary-Layer Equations Including Foreign Gas Injection," NASA TN D-5516, Nov. 1969.

[12] Hung, C.M. and MacCormack, R.W., "Numerical Solutions of Supersonic and Hypersonic Laminar Compression Corner Flows," *AIAA Journal,* Vol. 14, April 1976, pp. 475-481.

[13] MacCormack, R.W., "A Rapid Solver for Hyperbolic Systems of Equations," *5th International Conference on Numerical Methods in Fluid Dynamics,* June 28-July 2, 1976, Twente University of Technology, Enschede, The Netherlands.

[14] Horstman, C.C., "A Turbulence Model for Nonequilibrium Adverse Pressure Gradient Flows," *AIAA Journal,* Vol. 15, Feb. 1977, pp. 131-132.

[15] Glushko, G.S., "Turbulent Boundary Layer on a Flat Plate in an Incompressible Fluid," *Bulletin of the Academy of Science USSR,* Mechanics Series, No. 4, April 1965, pp. 13-23.

[16] Rubesin, M.W., "A One-Equation Model of Turbulence for Use with the Compressible Navier-Stokes Equations," NASA TM X-73, 128, April 1976.

[17] Viegas, J.R. and Coakley, T.J., "Numerical Investigation of Turbulence Models for Shock Separated Boundary-Layer Flows," AIAA Paper 7-44, Los Angeles, Calif., Jan. 1977.

[18] Settles, G.S., Bogdonoff, S.M., and Vas, I.E., "Incipient Separation of a Supersonic Turbulent Boundary Layer at High Reynolds Numbers," *AIAA Journal,* Vol. 14, Jan. 1976, pp. 50-56.